

Morphology and mobility of synthetic colloidal aggregates

Anastasios D. Melas^{a,b,*}, Lorenzo Isella^c, Athanasios G. Konstandopoulos^{b,d}, Yannis Drossinos^a

^a*European Commission, Joint Research Centre, I-21027 Ispra (VA), Italy*

^b*Department of Chemical Engineering, Aristotle University, GR-54124 Thessaloniki, Greece*

^c*European Commission, DG Energy, L-2530 Luxembourg, Luxembourg*

^d*Aerosol & Particle Technology Laboratory, CERTH/CPERI, P.O. Box 60361, GR-57001 Thessaloniki, Greece*

Abstract

The relationship between geometric and dynamic properties of fractal-like aggregates is studied in the continuum mass and momentum-transfer regimes. The synthetic aggregates were generated by a cluster-cluster aggregation algorithm. The analysis of their morphological features suggests that the fractal dimension is a descriptor of a cluster's large-scale structure, whereas the fractal prefactor is a local-structure indicator. For a constant fractal dimension, the prefactor becomes also an indicator of a cluster's shape anisotropy. The hydrodynamic radius of orientationally averaged aggregates was calculated via molecule-aggregate collision rates determined from the solution of a Laplace equation. An empirical expression that relates the aggregate hydrodynamic radius to its radius of gyration and the number of primary particles is proposed. The suggested expression depends only on

*Corresponding author.

Email address: admelas@auth.gr (Anastasios D. Melas)

geometrical quantities, being independent of statistical (ensemble-averaged) properties like the fractal dimension and prefactor. Hydrodynamic radius predictions for a variety of fractal-like aggregates are in very good agreement with predictions of other methods and literature values. Aggregate dynamic shape factors and DLCA individual monomer hydrodynamic shielding factors are also calculated.

Keywords: Power-law aggregates, fractal dimension, fractal prefactor, shape anisotropy, hydrodynamic radius, radius of gyration.

1. Introduction

Aerosol and colloidal particles may form complex structures via agglomeration [1] and flocculation. The morphology and hydrodynamic properties of these structures have been studied extensively in the literature, e.g., Refs. [2, 3], due to their numerous technological applications: for example, the mobility of power-law aggregates influences their size distribution, their precipitation behaviour, and their agglomeration. Even though many studies have investigated the relationship between geometric and dynamic properties, the prediction of the hydrodynamic radius from aggregate structural properties remains elusive.

Forrest and Witten [4], in their analysis of the agglomeration of ultrafine smoke particles, first suggested that the resulting agglomerates are power-law objects obeying the scaling law (over a finite size range)

$$N = k_f \left(\frac{R_g}{R_1} \right)^{d_f}, \quad (1)$$

where N is the number of primary particles that form the aggregate, d_f the fractal (or Hausdorff) dimension, k_f the fractal prefactor (also referred to

as lacunarity [5] or structure factor [6]), R_g the radius of gyration, and R_1 the radius of the primary particles. We refer to aggregates satisfying the scaling law Eq. (1) as “power-law” aggregates [7] (equivalently, fractal-like or quasi-fractal) because the scaling law relation is independent of whether the aggregate has a real scale-invariant (self-similar) morphology. The fractal dimension provides a quantitative measure of the degree to which a structure fills physical space beyond its topological dimension. The fractal prefactor, a parameter whose importance is increasingly being appreciated [6, 8, 9, 10], is an essential ingredient for a complete description of a power-law aggregate, as suggested by the scaling law. According to Wu and Friedlander [8] it is a descriptor of packing of the primary particles, becoming an indicator of the aggregate local structure. The radius of gyration is a geometric measure of the spatial mass distribution about the aggregate center of mass.

The calculation of the Stokes friction coefficient of a fractal-like aggregate, and consequently of its hydrodynamic radius, is analytically and computationally demanding as it requires the solution, analytical or numerical, of the creeping-flow Stokes equations. The hydrodynamic radius of an aggregate is defined as the radius of a sphere with the same mobility (or equivalently, the same diffusion coefficient) under identical flow conditions, ensemble-averaged over many aggregates and orientationally averaged [8]. Several methods have been proposed to calculate it.

Kirkwood and Riseman [11] in their pioneering analysis of the translational diffusion coefficient of flexible macromolecules derived a purely geometrical expression for the polymer friction coefficient. The derived expression depends only on monomer-monomer distances in the chain. Their analysis

was based on a double average of the Oseen tensor, a tensor that describes the perturbed fluid velocity on a surface due to a point source: an initial average over the internal configurations of the chain is followed by an orientational average. Hubbard and Douglas [12] modified their analysis by avoiding the configurational pre-averaging approximation, retaining the angular average of the Oseen tensor. The remaining angular average corresponds to the physical average over the orientational Brownian motion of the aggregate. They realized that the orientationally averaged (spherically symmetric) Oseen tensor is the free-space Green's function of the Laplace operator. Thus, they concluded that the orientationally averaged hydrodynamic friction of an arbitrarily shaped Brownian particle may be obtained from the solution of a Laplace equation. Hogan and co-workers in a series of papers [13, 14, 15] calculated the so-called Smoluchowski radius, the point mass-transfer analogue of the hydrodynamic radius, via stochastic simulations of point mass-aggregate collision rate. Their calculations are, in a sense, equivalent to the discrete stochastic simulations of the Hubbard and Douglas [12] continuum approach. Filippov [16] avoided the previously described approximations, at the expense of significant numerical effort, by developing a full multipole expansion of the Stokes velocity field to obtain the fluid stress tensor on the aggregate surface. The friction coefficient was subsequently calculated by integrating the stress tensor over the aggregate surface.

In this study we use the methodology introduced and validated by Isella and Drossinos [17] who calculated, approximately but accurately, the friction coefficient and the hydrodynamic radius of straight chains by solving a Laplace equation with appropriate boundary conditions. Their approach

is similar to the continuum approach of Hubbard and Douglas [12] and the single-particle discrete simulations performed by Hogan and collaborators [14]. Its advantages are the numerical solution of a simpler equation and easy computational implementation. The method as originally proposed is limited to colloidal aggregates or aerosol particles where mass and momentum transfer occurs in the so-called continuum regime. In the continuum transfer regime rarefaction effects, quantifiable by the Knudsen number, $\text{Kn} = \lambda/R_1$ where λ is the gas mean free path, are negligible as $R_1 \gg \lambda$ ($\text{Kn} = 0$).

The power-law aggregates we use in this work are synthetic in that they were generated by an algorithm that does not simulate a physical agglomeration mechanism. Instead, the algorithm allows the construction of power-law aggregates with specific properties. In the following, we study the morphology of these synthetic aggregates in an attempt to identify the geometrical factors that determine their small- and large-scale structure. We propose an empirical fit that relates their dynamical properties (hydrodynamic radius) to structural properties (radius of gyration).

2. Hydrodynamic radius of synthetic fractal-like aggregates

2.1. Methodology

In the continuum regime the Stokes friction coefficient of a N -monomer aggregate is [2]

$$f_N = \frac{1}{B_N} = \frac{k_B T}{D_N} \equiv 6\pi\mu R_h, \quad (2)$$

where B_N is the aggregate mechanical mobility, D_N the Stokes-Einstein diffusion coefficient, k_B the Boltzmann constant, μ the fluid viscosity, and R_h

the hydrodynamic radius. Equation (2) defines the aggregate hydrodynamic radius, which equals the mobility radius in the continuum regime.

Isella and Drossinos [17] argued that the ratio of two aggregate-to-monomer friction coefficients, and correspondingly of their hydrodynamic radii, is related to a ratio of two molecular collision rates: the molecular collision rate with the N -aggregate (K_N) and the molecular collision rate with a monomer (K_1). Accordingly,

$$\frac{f_N}{Nf_1} = \frac{K_N}{NK_1} = \frac{R_h}{NR_1}. \quad (3)$$

The collision rates may be calculated from the steady-state molecular diffusion equation [$\nabla^2\rho(\mathbf{r}) = 0$], via integrating the molecular diffusive flux $\mathbf{J}_N = -D_g\nabla\rho$ over the aggregate surface, where D_g is the molecular diffusion coefficient and ρ the gas density. The appropriate boundary conditions are total absorption on the aggregate surface [$\rho(\mathbf{r}_{\text{sur}}) = 0$, i.e., neglect of multiple scattering events] and constant fluid density far away from the aggregate ($\rho \rightarrow \rho_\infty$ for $|\mathbf{r}| \rightarrow \infty$). For a monomer, the molecular collision rate evaluates to $K_1 = 4\pi D_g R_1 \rho_\infty$. Thus, the friction coefficient may be determined from the numerical solution of a diffusion equation. For the diffusion calculations we used the finite-element software COMSOL Multiphysics [18].

Isella and Drossinos [17] validated the methodology for straight chains ($d_f = 1, k_f = \sqrt{3}$) by solving the diffusion equation in cylindrical coordinates. We reproduced their calculations in three-dimensional spherical coordinates. The size of the spherical computational domain was chosen to be at least two orders of magnitude larger than a characteristic dimension of the aggregate to ensure that the condition $\rho_\infty = \text{constant}$ hold at the computational-domain boundaries. We also tested the mesh-independence of the solutions. Figure 1

shows a power-law aggregate with the corresponding normal diffusive flux, whose integral over the aggregate surface gives the molecule-aggregate collision rate. The aggregate hydrodynamic radius is obtained through Eq. (3) and the appropriate normalization via K_1 .

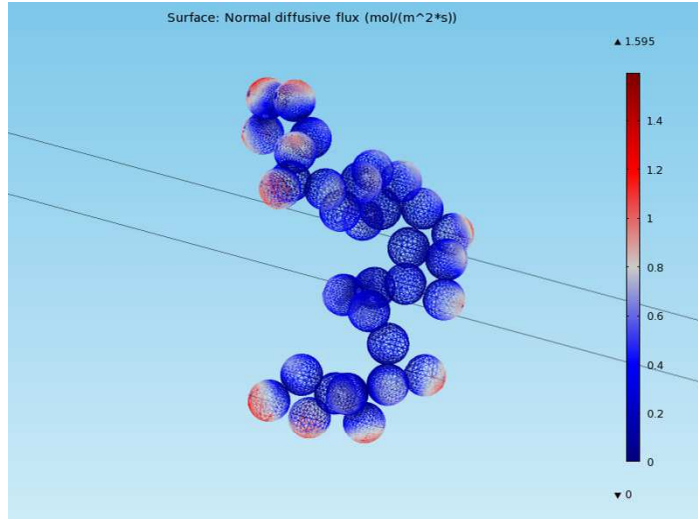


Figure 1: Normal diffusive flux on the surface of a DLCA ($d_f = 1.8, k_f = 1.3$) synthetic 32-monomer power-law aggregate.

Furthermore, we validated our calculations for two three-dimensional objects by comparing them to literature values. We calculated the perpendicular friction coefficient of two 3d, symmetric shapes composed of 8 particles: a cube and a rectangle. Our results are compared to the numerically evaluated, analytical calculations of Filippov [16] in Table 1. The highly accurate collision-rate results provide additional support that the method is general enough to be extended to power-law aggregates (with $d_f \neq 1$).

Table 1: Perpendicular friction coefficient of two 8-monomer symmetric objects.

Structure	Filippov [16]	Collision rate
Cube ($2 \times 2 \times 2$)	0.293	0.290
Rectangle ($2 \times 4 \times 1$)	0.361	0.366

2.2. Generation

The power-law aggregates used in our simulations were created with the tunable cluster-cluster aggregation algorithm proposed by Thouy and Julien [19] and modified by Filippov et al. [20]. The use of a “mimicking” algorithm, i.e., an algorithm that is not based on a physical agglomeration mechanism, allows us to generate aggregates that have prescribed number of primary particles, fractal dimension, and fractal prefactor. The synthetic aggregates satisfy exactly the scaling law by construction. They share many features with aggregates generated by physical process-based algorithms, and, more importantly, they provide an ensemble of well characterized aggregates to investigate the relationship between their static and dynamic properties.

We consider equal-sized, spherical, and non-overlapping monomers (primary particles). The creation of a fractal-like object starts by specifying the desired total number of primary particles $N = 2^n$ where n is the number of generations. Initially we create $N/2$ dimers; the dimers stick together to form 4-mers by choosing randomly a sticking point and a sticking angle, a process that guarantees that each aggregate is unique. This procedure continues for the n generations. The method is hierarchical as only clusters that have the same number of primary particles are used in each step. We generated

clusters composed of up to 4096 monomers with different d_f and k_f .

Most of the clusters we examined were created with parameters¹ characteristic of aggregates generated by Diffusion Limited Cluster Aggregation - DLCA (1.8, 1.3) [21] or Reaction Limited Cluster Aggregation - RLCA (2.05, 0.94) [22]. The agglomeration mechanism for both groups is diffusion, the difference arising from the cluster-monomer sticking probability: it is unity for DLCA clusters and 10^{-3} for RLCA [23]. Note that Ref. [22] uses (1.85, 1.117) for DLCA-like clusters.

The morphology of the generated structures was analyzed to ensure that they have the prescribed properties. A double logarithmic plot of the number of monomers versus the corresponding aggregate radius of gyration [Eq. (4)] for clusters composed of $N = 2^n$, $n = 8 - 12$ monomers and fixed (d_f, k_f) confirmed that the aggregates satisfy exactly the scaling law. The radius of gyration for N equal, spherical monomers is calculated by

$$R_g^2 = \frac{1}{N} \sum_{i=1}^N (\mathbf{r}_i - \mathbf{R}_{CM})^2 + \frac{3}{5} R_1^2, \quad (4)$$

where \mathbf{r}_i is the position of the i th monomer's center, and the aggregate center of mass is $\mathbf{R}_{CM} = 1/N \sum_{i=1}^N \mathbf{r}_i$. Note that we included the additive term $3R_1^2/5$ because we are interested in the power-law dependence even for small clusters; otherwise Eq. (4) evaluates to zero for a monomer. This additional term may also be taken to be the square of the monomer radius [16, 24]. We chose $3R_1^2/5$ because it is the radius of gyration of a single 3d sphere of radius R_1 [5, 10].² Of course, for large N the choice of the additional additive term

¹Henceforth, we shall specify power-law clusters by the ordered pair (d_f, k_f) .

²We repeated our calculations using R_1^2 as the additive term. We found minimal dif-

is irrelevant.

An alternative, more precise, validation method of the “mimicking” algorithm is based on the two-point, orientationally-averaged monomer-monomer correlation function $g(r)$. We calculated it as follows: an ensemble of M clusters composed of N monomers was generated, and all the pairwise (i, j) Euclidean distances were determined ($i, j = 1, \dots, N$). The total number of distances is $N(N-1)$. The number of particles $n_i(r)$ (equal to the number of distances) within the interval $[r - dr, r + dr]$ was recorded. We chose $dr = 0.1R_1$, a value we found to give reasonably smooth results [25]. The orientationally averaged, spherically symmetric pair correlation function is [20, 25]

$$g(r) = \frac{1}{M} \sum_{i=1}^M \frac{n_i(r)}{4\pi r^2 dr N}, \quad (5)$$

with the normalization condition

$$N - 1 = 4\pi \int_0^\infty dr r^2 g(r). \quad (6)$$

The physical interpretation of $g(r)$ is that it gives the probability (per unit volume) of finding a monomer at distance r from an arbitrarily chosen monomer [26]. Note that the pair correlation function, defined with respect to an arbitrarily chosen monomer, is distinct from the radial (mass) distribution function $\rho(r)$ which gives the cluster (mass) distribution with respect to its center of mass.

An analytic expression for $g(r)$ is highly desirable as structural and dynamical aggregate properties may be expressed in terms of it. The expected

ferences in the structural and dynamical properties of the generated clusters, even though the numerical constants in Eqs. (14, 15) differed slightly.

functional form is

$$g(r) = \frac{A}{R_1^{d_f}} r^{d_f-3} h\left(\frac{r}{\xi}\right), \quad (7)$$

where A is a constant. The algebraic decay arises from the scaling behaviour, and the cut-off function $h(r/\xi)$ models finite-size effects. The correlation length ξ is a measure of the cluster's diffuse interface, the interface ‘‘roughness’’. The cut-off function is usually taken to be a stretched exponential,

$$h\left(\frac{r}{\xi}\right) = \exp\left[-\left(\frac{r}{\xi}\right)^\gamma\right], \quad (8)$$

the stretching exponent γ at most weakly dependent on the agglomeration mechanism. As values are given $\gamma = 2.02$ [26] or 2.20 [25] for DLCA, and 2.16 for RLCA clusters [25]. The normalized, dimensionless pair correlation function $R_1^3 g(r/R_1)$ averaged over 2000 aggregates consisting of 512 monomers is plotted in Fig. 2: the left subfigure refers to DLCA aggregates, the right to RLCA aggregates.

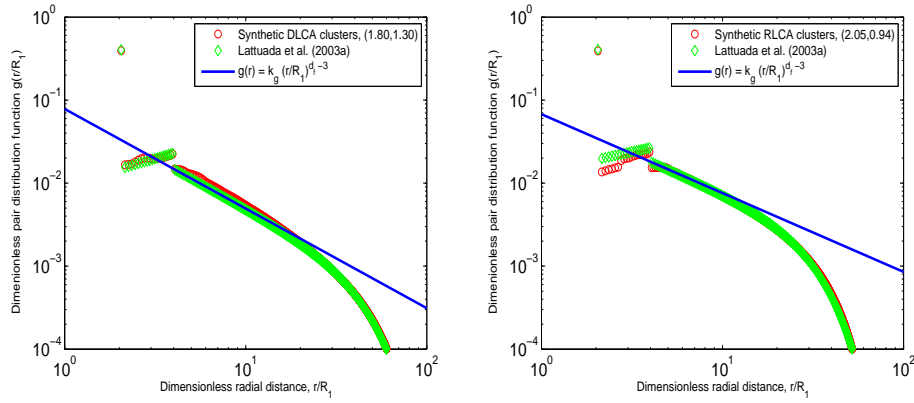


Figure 2: Normalized, dimensionless, spherically symmetric two-point correlation function ensemble-averaged over 2000 clusters with 512 monomers. Left: DLCA clusters, $k_g = 0.0782$; Right: RLCA clusters, $k_g = 0.0675$.

The most accurate expression, so far, for $g(r)$ has been proposed by Latuada et al. [22] who appreciated the importance of small-scale structure by identifying specific functional forms at the first and second shells ($r = 2R_1$ and $2R_1 < r < 4R_1$). The figure compares our results (“Synthetic clusters”) to theirs. The agreement is very good suggesting that the synthetic clusters exhibit the expected power-law decay with the specified fractal exponent ($d_f = 1.80$, left, and $d_f = 2.05$, right) over approximately one decade (compare to the pure scaling-law expression, solid line). The constant k_g in the pure algebraic-decay expression was evaluated as suggested in Ref. [22] (their constant c).

2.3. Scaling law

The scaling law Eq. (1) may also be re-written in terms of other characteristic length scales, like the outer radius R_{out} and the geometric radius R_{geo} . The outer radius is defined as half the maximum distance between any two monomers in the aggregate, whereas the geometric radius is the radius of the smallest sphere encompassing the aggregate, centered at its center of mass (the smallest convex envelope of the aggregate).³ Literature values for the ratio R_{out}/R_g , a ratio that can be used to determine the radius of gyration from TEM images [9], vary by about 20% for DLCA clusters, being in the range [1.45 – 1.65]. We analyzed ensembles of 5000 clusters consisting of up to 300 monomers to find that the ratio falls in the range [1.625 – 1.68]

³As the distance between monomers is calculated with respect to the monomers center of mass, the monomer radius R_1 has been added to the calculation of both length scales to ensure the correct single-monomer limit.

(DLCA) and $[1.625 - 1.69]$ (RLCA), cf. Fig. S1 (Supplementary Material), the ratio depending weakly on N . For approximately 100 monomers the ratio evaluates to ~ 1.675 (DLCA) and 1.685 (RLCA). The ratio $R_{\text{out}}/R_{\text{geo}}$ was determined to be 0.915 for both DLCA and RLCA synthetic clusters, largely independent of the number of monomers, cf. Fig. S2 (Supplementary Material).

We found, by performing linear fits on appropriate $\log N - \log R$ plots, that the fractal dimension does not depend on the chosen geometric length scale, whereas the prefactor does. In the case of the outer radius the prefactor is related to the average cluster packing fraction ϕ [26], while for the the geometric radius it becomes the inverse of the volume filling factor f [27]. The fractal-like scaling law remains valid even if expressed in terms of the hydrodynamic radius, as shown in Section 4.3; however, the exponent, referred to as the mass-mobility exponent, differs from the fractal exponent used in Eq. (1).

It is important to note, as inspection of Fig. 2 shows, that the aggregates considered herein are self-similar over a limited range of monomer-monomer distances. In particular, smaller clusters are not self similar and larger clusters have a diffuse interface. Nevertheless, the fractal-like scaling law is valid for a number of choices of the characteristic length scale, be it R_g , as in Eq. (1), R_{out} , or R_{geo} (or even the hydrodynamic radius, cf. Sec. 4.3); the validity of the scaling law for the synthetic clusters is reflected in referring to them as power-law or fractal-like. We use the scaling law irrespective of whether the aggregate has a real scale-invariant (self-similar) morphology. This implies that we approximate an aggregate by an aggregate with a sharp

interface [$\gamma \rightarrow \infty$, see Eq. (8)] for which the scaling law holds with respect to a well defined, outer length scale.

3. Fractal dimension (d_f) and prefactor (k_f)

3.1. Small-scale structure

The complex, and intricate, interdependence of N , d_f and k_f , and the resulting changes in the small- and large-scale structural properties of the aggregates, were investigated by examining ensembles of 5000 aggregates. The parameter choices and the calculated structural parameters are summarized in Table 2. Different cluster ensembles are grouped according to the parameter that is investigated (in bold): number of monomers (top group), fractal dimension (middle group), and fractal prefactor (last group). Note that 64-monomer clusters defined by (1.9, 1.3) and (1.8, 1.6) have identical radii of gyration.

An indicator of a cluster's small-scale structure is the probability distribution of the angles formed by three monomers. The angles are specified by two intersecting lines passing through the center of mass of a central monomer i and two j, k monomers touching it. For every monomer i we calculated the number of its neighbours k , to which we associated $k(k-1)/2$ angles (possible pairwise combinations). We calculated the angles from the distance d_{jk} of any two (j, k) pairs via

$$\theta_{ijk} = 2 \sin^{-1} \left(\frac{d_{jk}}{4R_1} \right). \quad (9)$$

Figure 3 presents the resulting distributions of three-monomer angles. The angles vary from 60° , the minimum possible angle for three touching equal-sized spheres their centers forming an equilateral triangle, and 180° , a locally

Table 2: Mean characteristic structural parameters: shape anisotropy $\langle A_{13} \rangle$ and three-monomer angle $\langle \theta_{ijk} \rangle$.

	N	(d_f, k_f)	R_g/R_1	$\langle A_{13} \rangle$	$\langle \theta_{ijk} \rangle$
1	512	(1.8, 1.3)	27.7	3.82	107.4
2	256	(1.8, 1.3)	18.8	3.77	107.3
3	128	(1.8, 1.3)	12.8	3.70	107.3
4	64	(1.8, 1.3)	8.7	3.69	107.2
4-bis	32	(1.8, 1.3)	5.93	3.69	106.9
4	64	(1.8, 1.3)	8.7	3.69	107.2
5	64	(1.9, 1.3)	7.8	3.23	105.4
6	64	(2.0, 1.3)	7.0	2.90	103.8
7	64	(2.1, 1.3)	6.4	2.60	102.4
4	64	(1.8, 1.3)	8.7	3.69	107.2
8	64	(1.8, 1.6)	7.8	3.52	102.6
9	64	(1.8, 1.9)	7.1	3.40	98.8
10	64	(1.8, 2.2)	6.5	3.30	92.6

straight chain configuration. Angles less than 60° would imply monomer overlapping or “necking”. The mean values reported in Table 2 (upper group) are in reasonable agreement with the previously reported value [25] for trimer distributions of (1.85, 1.117) DLCA aggregates, 103.57° . The distributions are independent of N , while they depend weakly on d_f and strongly on k_f . We note that as the prefactor increases the number of small angles ($\leq 80^\circ$) increases, suggesting that the prefactor is an indicator of local structure; for

fixed d_f as the prefactor increases the cluster becomes more locally compact ($\langle \theta_{ijk} \rangle$ decreases). This observation is also supported by the mean angles presented in Table 2, and the quantitative comparison presented in Table S1 (Supplementary Material).

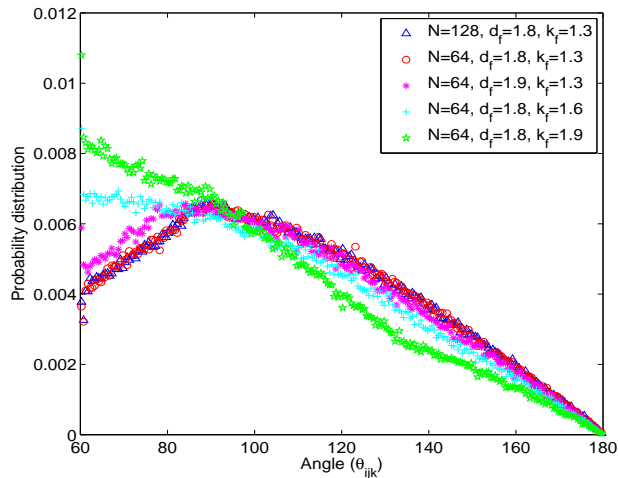


Figure 3: Ensemble-averaged probability distributions of three-monomer cluster angles.

An alternative indicator of local compactness is the mean number of nearest neighbors (number of touching monomers), or coordination number c_N , defined as the average number of contacts a monomer has within an aggregate [2]. The cluster coordination number not only provides information on the openness of an aggregate and its compactness, but it is a factor that influences monomer hydrodynamic shielding within an aggregate [28]. Reference [24] used the coordination number as an indicator of cluster compactness, albeit for clusters generated by a completely different, physically-based agglomeration mechanism. For the synthetic fractals analyzed herein, i.e., generated by the cluster-cluster aggregation algorithm, Gastaldi and

Vanni [29] argued that the the coordination number is

$$c_N = 2 \frac{N - 1}{N}. \quad (10)$$

We checked this expression for clusters composed of $N = 16, 32, 64, 128$ with different (d_f, k_f) : we found it to be very accurate. Figures S3 and S4 (Supplementary Material) present probability distributions of the number of nearest neighbours for cluster ensembles specified by $N = 64, 128$, $d_f = 1.5, 1.8$ and $k_f = 1.3, 2.2$. As the prefactor increases the distribution function broadens, but the coordination number is only a function of the number of monomers, as suggested by Eq. (10).

3.2. Large-scale structure

One recently used large-scale indicator is the cluster shape anisotropy A_{13} , a measure of cluster stringiness; for example, as A_{13} increases the aggregate becomes more cigar-like. The shape anisotropy is calculated from the principal radii of gyration R_i ($i = 1, 2, 3$) by diagonalizing the aggregate inertia tensor [30]. Accordingly, the radius of gyration may be written as [26]

$$R_g^2 = \frac{1}{2}(R_1^2 + R_2^2 + R_3^2), \quad R_1 \geq R_2 \geq R_3, \quad (11)$$

and the shape anisotropy A_{13} is defined by

$$A_{13} = \frac{R_1^2}{R_3^2}. \quad (12)$$

Figure 4 presents probability distributions of shape anisotropies for different ensembles of fractals. We observe that A_{13} depends strongly on d_f , weakly on k_f , and is independent of N . These observations are confirmed by the mean $\langle A_{13} \rangle$ reported in Table 2. We remark that anisotropies extend

over a large range of values, even for the same (d_f, k_f) . As expected, our results agree with Thouy and Jullien [31], who concluded that (for fixed k_f) shape anisotropy is independent of N and dependent on d_f .

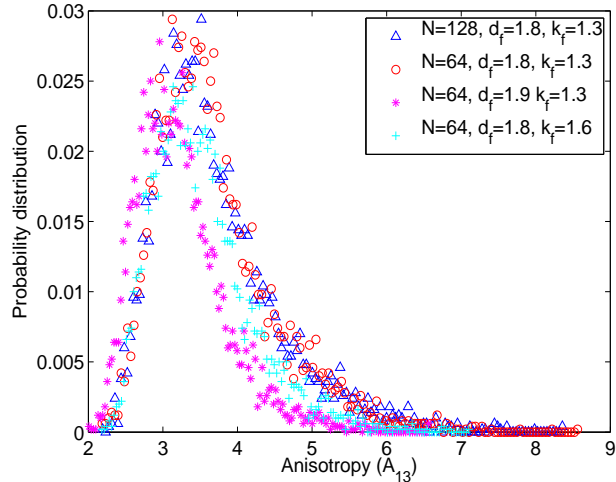


Figure 4: Probability distribution of shape anisotropy A_{13} .

It is worthwhile to compare our results to Heinson et al. [26, 30] who argued that shape anisotropy affects the prefactor, rendering k_f a shape indicator. Our results are in agreement on the importance of the prefactor as descriptor of an aggregate morphology: in fact, we identify synthetic clusters by the ordered pair (d_f, k_f) , and the calculated mean shape anisotropy for DLCA fractals (Table 2, upper group) is in reasonable agreement with their reported value $\langle A_{13} \rangle = 3.86$ [26]. Moreover, we find that, for *fixed* d_f , the prefactor k_f depends on the mean anisotropy, albeit weakly. Since the synthetic clusters are generated by specifying the fractal prefactor, the argument that $\langle A_{13} \rangle$, via the prefactor, describes aggregate structure at large length scales, may be inverted, emphasizing the importance of k_f to deter-

mine $\langle A_{13} \rangle$. For fixed fractal dimension, the two approaches are equivalent, i.e., if $\langle A_{13} \rangle$ increases k_f decreases and vice versa, suggesting that local structure has an effect on large-scale structure and vice versa. If, however, d_f is allowed to change we find that the effect of its change on the shape anisotropy distribution (and, specifically, on its mean) is more important than the effect of a change of the prefactor.

These observations on the effect of structural parameters on aggregate morphology are summarized in Table 2. A comparison of clusters pertaining to the middle group shows the effect of d_f , whereas a comparison of the lower group shows the effect of k_f . They indicate that changes of the fractal dimension produce larger changes of the mean shape anisotropy, and changes of the prefactor larger changes of the mean three-monomer angles. The comparisons are rendered quantitative in Table S1 (Supplementary Material), where the effect of variations of the scaling-law parameters d_f, k_f and the number of monomers N on mean characteristic cluster structural parameters is presented as appropriate percentage changes.

Hence, in general, the fractal dimension is an indicator of the overall aggregate shape (large-scale aggregate morphology), while the prefactor becomes an indicator of local structure (small-scale morphology). Mean shape anisotropy (an indicator of the aggregate shape) is important as it affects the value of the prefactor.

4. Aggregate structure and hydrodynamic radius

4.1. Dependence of the hydrodynamic radius on the radius of gyration

We calculated the hydrodynamic radii of clusters composed of 8, 16, 32, 64 primary particles with (d_f, k_f) in the ranges $([1.5, 2.1], [1, 1.6])$. We simulated three realizations of nine different (d_f, k_f) pairs for each N . Calculated hydrodynamic radii are plotted against the corresponding radii of gyration in Fig. 5. Each symbol represents a single aggregate.

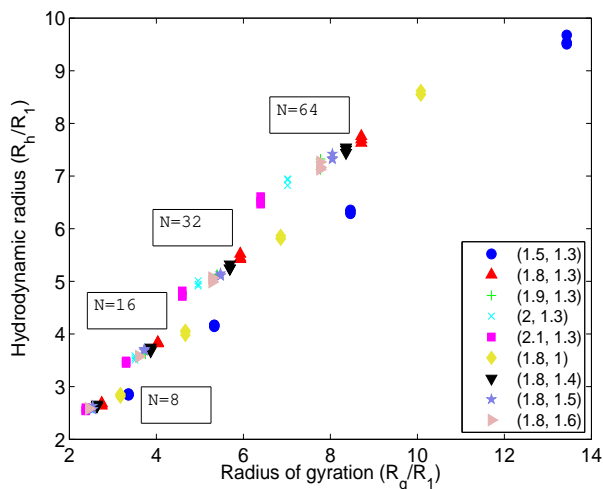


Figure 5: Hydrodynamic radius as a function of the radius of gyration.

A striking feature of the figure is that the calculated R_h cluster according to the number of monomers, suggesting a linear (R_h, R_g) relationship for a given monomer number. Accordingly, for fixed N , we fit linearly the data to

$$\frac{R_h}{R_1} = m(N) \frac{R_g}{R_1} + b(N), \quad (13)$$

the slope m and the y -intercept b being functions of N . The resulting four $m(N)$ and $b(N)$ are averaged to obtain the final empirical fit. In fact, we

performed two different fits: one with the independent variable being the equivalent volume radius ($R_{eq} = R_1 N^{1/3}$)

$$\frac{R_h}{R_1} = 0.248 \left(2 - N^{-1/3} \right) \frac{R_g}{R_1} + 0.69 N^{0.415}, \quad (14)$$

and one with $\ln(2N)$, a dependence suggested by the (R_h, R_g) relationship for straight chains (see, for example, Ref. [17]),

$$\frac{R_h}{R_1} = 0.548 \left[1 - \frac{1}{\ln(2N)} \right] \frac{R_g}{R_1} + 0.73 N^{0.40}. \quad (15)$$

Since the numerical fits were obtained from three different (N, d_f, k_f) realizations [corresponding, nevertheless, to $27 \times 4 = 108$ (N, R_g) realizations], we estimated the variability of the hydrodynamic radius for two (N, d_f, k_f) choices. We calculated the hydrodynamic radius of 10 DLCA and 10 RLCA clusters to obtain the mean hydrodynamic radius, $\langle R_h \rangle$, and an estimate of the hydrodynamic-radius variability, herein chosen to be the ratio of the hydrodynamic radius standard deviation to the mean hydrodynamic radius, $\sigma_{R_h} / \langle R_h \rangle$ (expressed as a percentage). Results are shown in Fig. 6. The left subfigure presents the calculated hydrodynamic radii for each cluster realization and the numerical fit: the agreement is very good. Note that the hydrodynamic-radius variability is so small that error bars would not have been visible. The right subfigure presents the chosen measure of the variability. It is important to note that the variability of R_h is so small that even a limited number of (N, d_f, k_f) triplet realizations would cover a large range of R_h values, thereby justifying our choice to use a limited number of triplets.

Equations (14, 15) suggest that neither the fractal dimension nor the fractal prefactor are separately necessary to estimate R_h , as it may be fitted solely on N , R_g (and, of course, R_1). The general dependence $R_h = f(N, k_f, d_f)$

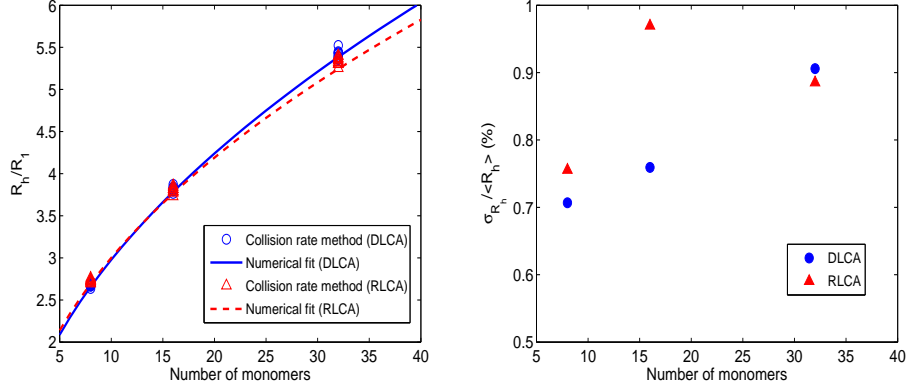


Figure 6: Left: Calculated hydrodynamic radii of 10 DLCA and 10 RLCA clusters (symbols). Comparison with numerical-fit predictions (lines); Right: Variability of DLCA and RLCA hydrodynamic radii: percentage ratio of the hydrodynamic-radius standard deviation to the mean hydrodynamic radius.

may, thus, be simplified via the implicit dependence on k_f and d_f through R_g , $R_h = f(N, R_g(N, k_f, d_f))$. This observation should be contrasted to most empirical fits in the literature where the hydrodynamic radius is expressed in terms of R_g , d_f , and possibly N see, for example, Refs. [15, 27]. Moreover, Eqs. (14, 15) imply that R_h may be calculated for a single cluster, if the monomer positions are known (from simulations or experimental measurements), since the independent variables do not depend on ensemble-averaged properties like d_f and k_f .

Henceforth, we will use Eq. (14) as the predicted hydrodynamic radii R_h are almost identical, irrespective of which equation is used. Figure 7 compares the numerically determined ratio R_h/R_g for up to $N = 1000$ to previously proposed theoretical [11], semi-analytical [27], and numerical [15, 32] expressions. The left subfigure refers to DLCA clusters, whereas the

right subfigure to RLCA clusters. Note that as $N \rightarrow \infty$ the ratio tends to a constant characteristic of the agglomeration mechanism.

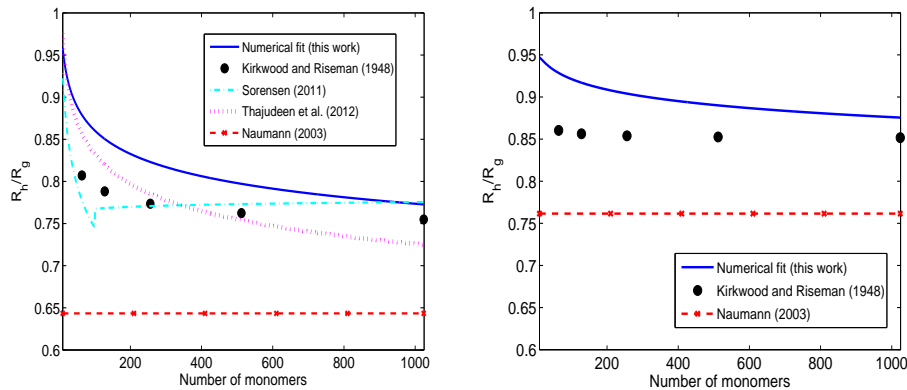


Figure 7: Comparison of predicted ratios of the hydrodynamic to the radius of gyration. Left: DLCA clusters; Right: RLCA clusters.

Our results compare favorably to the purely geometric expression derived by Kirkwood and Riseman [11], according to which

$$\frac{NR_1}{R_h} = 1 + \frac{1}{N} \sum_{j=1}^N \sum_{m=1, m \neq j}^N \frac{R_1}{|\mathbf{r}_j - \mathbf{r}_m|}. \quad (16)$$

Predictions of Eq. (16) are lower than the empirical-fit predictions for small aggregates, approaching the same limit as N increases. The comparison suggests that the Kirkwood-Riseman expression gives a very good approximation to the hydrodynamic radius of both open and closed structures, the difference increasing as the number of monomers decreases (as expected since it is a large N expression).

Our predictions are also compared to the recently suggested expression by Thajudeen et al. [15],

$$R_s \approx R_h = \frac{R_g}{\alpha_1(d_f) + \alpha_2(d_f)}, \quad (17)$$

where R_s is the Smoluchowski radius, taken to be approximately equal to the hydrodynamic radius (as in this work), and α_i ($i = 1, 2$) are quadratic functions of d_f . Note that Eq. (17) depends explicitly on d_f , and it has six fitting parameters. Its range of validity is $k_f = 1.3$ and d_f in the range $[1.30 - 2.60]$; hence, the calculation of the hydrodynamic radius of RLCA clusters is beyond its region of validity.

The fit proposed by Naumann [27] underestimates the ratio R_h/R_g . A possible reason is that R_h is expressed in terms of R_{geo} ; for our synthetic clusters $R_{\text{geo}}/R_g = 1.83$ (DLCA) and 1.84 (RLCA) (see Section 2.3) values different from the analytical expression $R_{\text{geo}}/R_g = [(d_f + 2)/d_f]^{1/2}$ that evaluates to 1.45 (DLCA) and 1.41 (RLCA). A larger ratio would result in larger R_h/R_g , closer to the collision-rate results.

Figure 7 also compares our DLCA results to the expression proposed in the recent review of the mobility of fractal aggregates [32]. The suggested expression is a piece-wise continuous function, the segments matching at $N = 100$, but with a crossover at $N = 74$.

Our results for the ratio R_h/R_g are also compared to available numerical calculations and experimental measurements for specific cluster parameters in Table 3. They differ from Filippov's calculations [16] by less than 10%, providing further support of the validity of our proposed expression. Latuada et al. [22] calculated of same ratio for fractals generated by a Monte Carlo cluster-cluster aggregation method via the Kirkwood-Riseman method. Again, the agreement is very good.

As an additional confirmation of the accuracy of our empirical expression we considered the 20 structures discussed in detail in Ref. [15], their

Table 3: Comparison of numerically determined ratio R_h/R_g with literature values.

	N	(d_f, k_f)	R_h/R_g	Eq. (14)
Fillipov [16]	100	(1.8, 1.3)	0.89	0.86
	100	(1.8, 2.3)	0.98	1.02
	100	(1.2, 2.5)	0.60	0.66
Lattuada	1000	(1.85, 1.117) DLCA	0.77	0.78
et al. [22]	1000	(2.05, 0.94) RLCA	0.83	0.88
Wang and	1000	(1.75, not specified)	0.7	0.74 ($k_f = 1.3$)
Sorensen [33]	1000	(2.15, not specified)	0.97	1.02 ($k_f = 1.3$)

Table 1. We found, Fig. 8, that predictions are in excellent agreement with the six-parameter fit, the differences being at maximum $\pm 5\%$. This result is not surprising as the two methodologies are very similar: the collision-rate methodology obtains the hydrodynamic radius from the solution of a diffusion equation, whereas the methodology used in Ref. [15] is based on averages of particle-trajectory properties calculated from the corresponding Langevin equations.

The proposed relationship between the hydrodynamic radius and the radius of gyration may be easily converted into an expression relating the hydrodynamic radius to the outer radius, a quantity sometimes easier to determine experimentally than the radius of gyration (see Section 2.3 for an estimate of R_{out}/R_g).

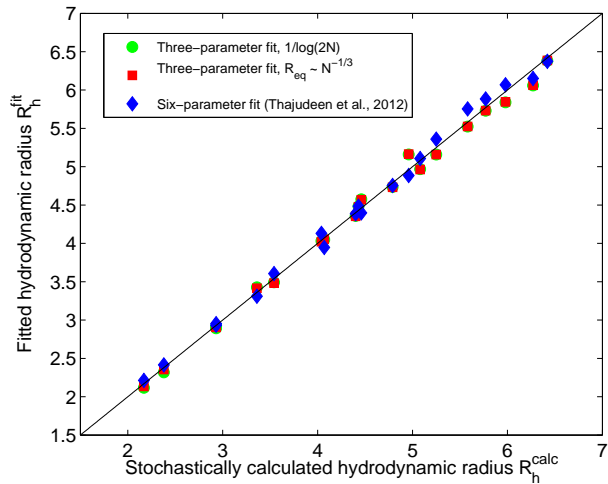


Figure 8: Comparison of two numerical fits, Eqs. (14, 15), to calculated hydrodynamic radii, Ref. [15].

4.2. Power-law aggregates generated by Langevin dynamics

An important feature of the proposed fit is that its application does not require explicitly the cluster statistical properties (ensemble averaged) d_f and k_f . The fitting parameters depend only on morphological (geometric) properties, as does the Kirkwood-Riseman expression. Consequently, it may be used to calculate the hydrodynamic radius of clusters given only their geometry.

A specific example of the usefulness of our numerical fit is provided by considering the power-law aggregates generated in Ref. [24]. These aggregates were generated by solving the Langevin equations of motion of a set of monomers interacting via a central potential in a quiescent fluid. The easily determined, instantaneous properties of these structures are geometric: the radius of gyration and the number of primary particles. The proposed fit pro-

vides an efficient formula to estimate the diffusion coefficient of aggregates as they are being formed, and thus to determine aggregate formation without relying on the so-called “free draining” approximation for the hydrodynamic shielding of monomers within a cluster.

We calculated the hydrodynamic radii by the collision-rate methodology, and we compare them to predictions of the Kirkwood-Riseman theory and the proposed expression Eq. (14) in Fig. 9. The very good agreement (maximum deviation 10%) indicates that our fit reproduces the hydrodynamic radii even for power-law aggregates generated by other methods. We note that due to the choice of a spherically symmetric monomer-monomer interaction potential, the Langevin-dynamics generated power-law aggregates were locally compact (large clusters at late time $k_f = 3.65$), and on larger scales tubular and elongated (large clusters at late time $d_f = 1.56$). Thus, the comparison provides a rather stringent test of the proposed expression. As for the small-cluster comparison shown in Fig. 7, the Kirkwood-Riseman expression provides a good approximation to the hydrodynamic radii, albeit slightly under-predicting them.

4.3. Mobility scaling law and dynamic shape factor

It has been argued that the scaling law remains valid even when the characteristic length scale is chosen to be the mobility radius (equal to the hydrodynamic radius in the continuum regime). The corresponding scaling law is

$$N = k_m \left(\frac{R_h}{R_1} \right)^{d_m}, \quad (18)$$

where d_m is the mass-mobility exponent. We fitted the hydrodynamic radius calculated for DLCA and RLCA aggregates to the number of primary

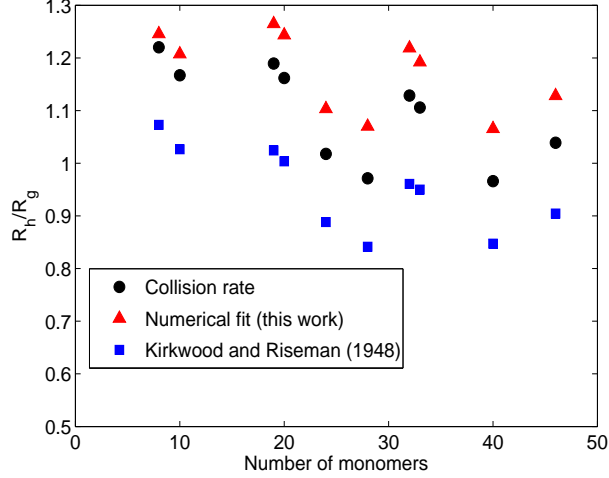


Figure 9: Ratio of the hydrodynamic radius to the radius of gyration for power-law aggregates generated via Langevin-dynamics simulations: Collision-rate calculation, numerical fit, and Kirkwood-Riseman predictions.

particles (log-log fit) to obtain

$$N = 1.17 \left(\frac{R_h}{R_1} \right)^{1.97}; \quad \text{DLCA (1.8, 1.3)}, \quad (19a)$$

$$N = 0.92 \left(\frac{R_h}{R_1} \right)^{2.14}; \quad \text{RLCA (2.05, 0.94)}. \quad (19b)$$

Thus, even though for different geometric radii the fractal dimension remains the same, when a dynamic length scale is used the fractal dimension changes [32, 34]. Of course, the corresponding fractal prefactors change.

The mass mobility exponent may be related to the fractal dimension by combining Eqs. (1, 18) to obtain

$$d_m = d_f \frac{\log R_g}{\log R_h} \left[1 + \frac{\log(k_f/k_m)}{d_f \log R_g} \right]. \quad (20)$$

We found that use of the proposed expression for the hydrodynamic radius in Eq. (20) reproduces d_m to within less than 0.5%. Moreover, the first term

on the right-hand-side approximates d_m to within 5% (DLCA) and 1.5% (RLCA). Note, however, that the difference between the calculated fractal dimension and the mass mobility dimension is 10% (DLCA) and 5% (RLCA).

Lastly, the empirical fit may be used to obtain the dynamic shape factor χ_N , a correction factor used to account for the effect of the aggregate shape on its motion. It becomes [17]

$$\chi_N = \frac{R_h}{R_1} N^{-1/3}. \quad (21)$$

Figure 10 presents the calculated values for both DLCA and RLCA clusters as a function of monomer number. The dynamic shape factor may also be

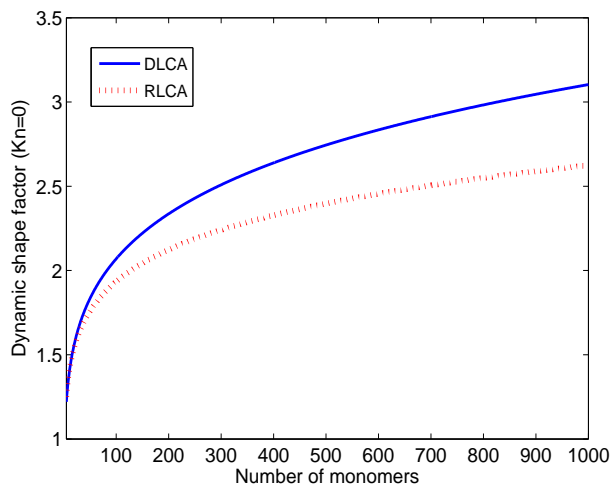


Figure 10: Calculated dynamic shape factor of DLCA and RLCA clusters.

used to define the cluster effective density, the density of a fictitious spherical particle of radius the hydrodynamic radius and of the same mass as the initial irregularly shaped aggregate. It is defined by

$$\rho_{\text{eff}} = \rho_1 N \left(\frac{R_1}{R_h} \right)^3. \quad (22)$$

where ρ_1 is the monomer material density. Equations (21, 22) lead to $\rho_{\text{eff}} = \rho_1/\chi_N^3$.

4.4. Dependence of the hydrodynamic radius on the mean number of nearest neighbours

The cluster hydrodynamic radius may be expressed in terms of the cluster average monomer shielding factor η_N or the individual i th monomer shielding factor $\eta_{N,i}$ via [17]

$$\frac{R_h}{R_1} = N \eta_N = \sum_{i=1}^N \eta_{N,i}. \quad (23)$$

The orientationally-averaged shielding factor, either average or individual, not only allows the explicit calculation of the hydrodynamic radius, but it has also been used to calculate a cluster's permeability and thereby its hydrodynamic radius [28, 35]. Short-range within-cluster interactions, which affect monomer shielding, were incorporated in the calculation of a cluster's permeability through the individual monomer local coordination number, i.e., the number of nearest neighbours of each monomer (number of touching monomers). Long-range effects were expressed in terms of the average volume fraction.

We used collision-rate simulations to calculate the average shielding factor. Results are shown in Table 4. We note that η_N depends not only on short-range effects, as modelled by the prefactor, but also on long-range effects, as described by the number of monomers and the fractal dimension. This observation is further supported by Eq. (14), where the importance of the number of monomers is explicit.

The influence of the *local* coordination number, namely the number of

Table 4: Average cluster shielding factor of clusters calculated by collision-rate simulations.

N	d_f	k_f	R_g/R_1	c_N , Eq. (10)	η_N
16	1.8	1.3	4.03	1.875	0.239
32	1.8	1.6	5.28	1.937	0.157
32	1.8	1.3	5.93	1.937	0.171
32	1.5	1.3	8.46	1.937	0.198

neighbours a chosen monomer has (and not the cluster average), on the average monomer shielding within an aggregate was further investigated by calculating the shielding factor of each monomer in a power-law aggregate. Figure 11 presents the collision-rate calculated individual-monomer shielding factors (averaged over very few clusters) as a function of the number of nearest neighbors for DLCA clusters composed of 8, 16, 32 monomers. These results, coupled to the probability distribution of nearest neighbours, may be used to calculate the average shielding factor. However, we note that the individual shielding factors do not fall on a “universal” (independent of N) line, but fall into three lines parametrized by the number of monomers in the aggregate. Thus, the $\eta_{N,i}$ shown in Fig. 11, being dependent on the overall number of monomers, may not be easily used to estimate the cluster friction coefficient (or permeability) of clusters composed of an arbitrary number of monomers. The results are consistent with the previously made observation that the shielding factor of a monomer depends on a short-range effect, expressed by the number of nearest neighbours, and a long-range effect related to the large-scale structure and the size of the cluster, as noted in

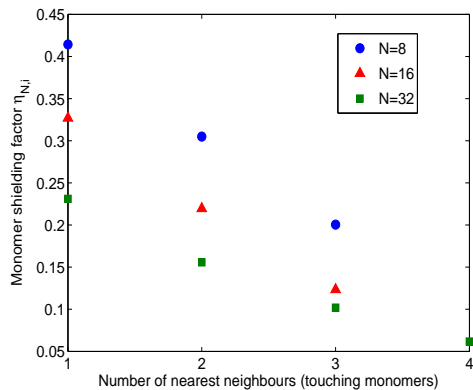


Figure 11: Individual-monomer shielding factors within DLCA clusters as a function of nearest neighbours (local coordination number).

Ref. [35].

5. Conclusions

The purpose of our study was to investigate the relationship between structural and dynamic properties of fractal-like aggregates in the continuum mass and momentum transfer regimes. We calculated the hydrodynamic radius of synthetic colloidal aggregates through the numerical solution of a diffusion equation with appropriate boundary conditions. The resulting normal diffusive flux was related to the molecule-aggregate collision rate and eventually to the aggregate friction coefficient. The power-law aggregates used in the simulations were generated via a cluster-cluster aggregation algorithm.

The morphology of the synthetic aggregates was analyzed via the three-monomer angle distribution, the mean number of nearest neighbours (monomers in the first coordination shell), and the distribution of cluster shape anisotropy. The large-scale distribution of monomers within a power-law aggregate is

mainly determined by the fractal dimension d_f , even though for fixed d_f , the mean shape anisotropy provides a good descriptor of aggregate morphology at large scales. The fractal prefactor k_f , dependent on the shape anisotropy, describes the local monomer distribution, as determined by the three-monomer angle distribution and the average number of nearest monomer neighbors.

The aggregate hydrodynamic radius R_h , equal to the mobility radius in the continuum regime, was related to the radius of gyration R_g and the number of primary particles (monomers) N via an empirical formula leading to $R_h(N, R_g(d_f, k_f, N); R_1)$. The suggested relationship shows the importance of both d_f and k_f in determining the dynamics of an aggregate; however, their individual values are not required separately since the hydrodynamic radius may be predicted through their combined effect as specified by the radius of gyration. Furthermore, since the proposed expression does not depend on statistical cluster properties (like d_f and k_f) it may be used to estimate the hydrodynamic radius of single fractal-like objects. Predictions of the suggested expression were in excellent agreement with literature values for a large range of different (d_f, k_f) pairs, and for aggregates generated by different methods, e.g., a “mimicking” algorithm or Langevin dynamics. These comparisons suggest that the validity of the expression is general enough to be used in different settings.

The hydrodynamic-radius expression was used to study the scaling law connecting the number of monomers to the hydrodynamic radius of DLCA (1.8, 1.3) and RLCA (2.05, 0.94) clusters. We found, in agreement with previous works, that the fractal exponent determined from the radius of gyration and the mass-mobility fractal dimension determined from the hydrodynamic

radius differed, suggesting that the hydrodynamic radius is not a linear function of the radius of gyration (as manifested by the proposed expression).

We, also, calculated the shielding factor of individual monomers in DLCA aggregates. Since the fractal dimension and prefactor were taken to be constant for DLCA clusters, the effect of the number of primary particles and probability distribution of nearest neighbours (considered as an indicator of a cluster's small-scale morphology) were studied. We found that the individual shielding factor, and consequently the cluster's hydrodynamic behaviour, depends on the combined effect of small- and large-scale structural properties, since both the number of nearest neighbours (local structure) and primary particles (large-scale structure) influence the shielding factors. Consequently, the pair (d_f, k_f) is required for a full characterization of both the structure and dynamics of a power-law aggregate.

References

- [1] S. di Stasio, A.G. Konstandopoulos, M. Kostoglou, *J. Colloid Interface Sci.* 247 (2002) 33.
- [2] S.K. Friedlander, *Smoke, Dust and Haze*, Oxford University Press, New York, 2000.
- [3] R. Jullien, R. Botet, *Aggregation and Fractal Aggregates*, World Scientific Publishing Co., Singapore, 1987.
- [4] S.R. Forrest, T.A. Witten, *J. Phys. A* 12 (1979) L109.
- [5] M. Lapuerta, F.J. Martos, and G. Martín González, *J. Colloid Interface Sci.* 346 (2010) 23.

- [6] L. Gmachowski, *J. Colloid Interface Sci.* 178 (1996) 80.
- [7] M.K. Wu, S.K. Friedlander, *J. Aerosol Sci.* 24 (1993) 273.
- [8] M.K. Wu, S.K. Friedlander, *J. Colloid Interface Sci.* 159 (1993) 246.
- [9] U.O. Köylü, Y. Xing, D.E. Rosner, *Langmuir* 11 (1995) 4848.
- [10] C.M. Sorensen, G.C. Roberts, *J. Colloid Interface Sci.* 186 (1997) 447.
- [11] J.G. Kirkwood, J. Riseman, *J. Chem. Phys.* 16 (1948) 565.
- [12] J.B. Hubbard, J.F. Douglas, *Phys. Rev. E* 47 (1993) R2983.
- [13] Gopalakrishanan, Hogan, *Aerosol Sci. Technol.* 45 (2011) 1499.
- [14] C. Zhang, T. Thajudeen, C. Larriba, T.E. Schwartzentruber, C.J. Hogan, *Aerosol Sci. Technol.* 46 (2012) 1065.
- [15] T. Thajudeen, R. Gopalakrishnan, C.J. Hogan, *Aerosol Sci. Technol.* 46 (2012) 1174.
- [16] A.V. Filippov, *J. Colloid Interface Sci.* 229 (2000) 184.
- [17] L. Isella, Y. Drossinos, *J. Colloid Interface Sci.* 356 (2011) 505.
- [18] Comsol Multiphysics, Chemical Engineering Module, version 3.5, <http://www.comsol.com/products/chem/> (2008).
- [19] R. Thouy, R. Jullien, *J. Phys. I France* 6 (1996) 1365.
- [20] A.V. Filippov, M. Zurita, D.E. Rosner, *J. Colloid Interface Sci.* 229 (2000) 261.

- [21] A.M. Brasil, T.L. Farias, M.G. Carvalho, *J. Aerosol Sci.* 33 (2000) 440.
- [22] M. Lattuada, H. Wu, M. Morbidelli, *J. Colloid Interface Sci.* 268 (2003) 96.
- [23] M. Lattuada, H. Wu, M. Morbidelli, *Chem. Eng. Sci.* 59 (2004) 4401.
- [24] L. Isella, Y. Drossinos, *Phys. Rev E* 82 (2010) 011404.
- [25] M. Lattuada, H. Wu and M. Morbidelli, *J. Colloid Interface Sci.* 268 (2003) 106.
- [26] W. R. Heinson, C. M. Sorensen, A. Chakrabarti, *J. Colloid Interface Sci.* 375 (2012) 65.
- [27] K. Naumann, *J. Aerosol Sci.* 34 (2003) 1371.
- [28] R.C. Sonntag, W.B. Russel, *J. Colloid Interface Sci.* 115 (1987) 378.
- [29] A. Gastaldi, M. Vanni, *J. Colloid Interface Sci.* 357 (2011) 18.
- [30] W.R. Heinson, C.M. Sorensen, A. Chakrabarti, *Aerosol Sci. Technol.* 44 (2010).
- [31] R. Thouy, and R. Jullien, *J. Phys. A* 30 (1997) 6725.
- [32] C. M. Sorensen, *Aerosol Sci. Technol.* 45 (2011) 755.
- [33] G.M. Wang, C.M. Sorensen, *Phys. Rev. E* 60 (1999) 3036.
- [34] L. Gmachowski, *Colloids and Surfaces A: Physicochem. Eng. Aspects* 211 (2002) 197.
- [35] M. Vanni, *Chem. Eng. Sci.* 55 (2000) 685.